COMPARATIVE NON-LINEAR SIMULATION OF TEMPERATURE PROFILES INDUCED IN AN EXHAUST MANIFOLD DURING COLD-STARTING

D.A. DESAI

ABSTRACT

The simulation of an exhaust manifold's thermal behaviour is an important concern for various reasons. Amongst them is the need to minimise catalyst light-off time as significant exhaust emissions are generated within this period. Modelling such behaviour is not simplistic as it is governed by complex interactions between exhaust gas flow and the manifold itself. Computational fluid dynamics (CFD) is a powerful tool for such simulations. However its applicability for transient simulations is limited by high central processing unit (CPU) demands. The present study proposes an alternative computational method to assess and rank the relative impact of the manifold's thermal properties on its exterior temperature. The results show that stainless steel manifolds potentially minimise heat loss from the exhaust gas when compared with their cast iron counterparts. This may result in an increase in thermal energy being available to heat the catalyst.

Keywords: Heat transfer modelling, exhaust manifold, engine cold-start, finite element analysis (FEA)

Nomenclature

c_p	heat capacity of pipe material (J/kg/K)
c_{pg}	specific heat of gas at constant pressure (J/kg/K)
d_1	pipe inner diameter (m)
d_2	pipe outer diameter (m)
f	frictional factor
g	gravitational acceleration (9.81 m/s^2)
h	heat transfer coefficient (W/m^2/K)
k	thermal conductivity (W/m/K)
$\dot{m}$	mass flow rate of exhaust gas (kg/s)
N_u	Nusselt number
Pr	Prandtl number
Q	heat transfer (J)
q	heat flux (w/m^2), heat loss (W)
Ra	Rayleigh number
Re	Reynolds number
S	surface area (m^2)
T	temperature (K)
t	time (s)
u	axial gas velocity (m/s)
x	axial coordinate of exhaust system (m)

Greek letters

α	thermal diffusivity (m^2/s)
β	volumetric thermal expansion coefficient (1/K)
ν	kinematic viscosity (m^2/s); velocity of fluid (m/s)
ρ	density (kg/m^3)
μ	dynamic viscosity (kg/ms)
σ	Stefan-Boltzmann constant (5.67 x 10^{-8} W/m^2 K^4)
ε	emissivity, surface roughness (m)
η	viscosity (m^2/s)

Subscripts

a	air
c	critical
cva	convection to ambient
eva	evaporation
f	film
g	gas
gp	convection between exhaust gas and pipe wall
p	pipe
rad	radiation

1. INTRODUCTION

Tailpipe emissions have been a strong consideration during the last 18 years when designing exhaust manifolds. In order to meet the current Euro 4 emission standards, the light-off time of the catalyst should be less than 40 seconds (s) after a cold start. This is perceived as difficult to achieve particularly for hydrocarbons (HC). Thermal inertia and heat loss through the exhaust manifold are main factors that could significantly influence the inlet gas temperature of the catalytic converter. Therefore, ongoing research efforts are directed towards optimising heat management and minimising the time taken to reach the appropriate catalyst operating temperature.

One of the major components impacted is the exhaust manifold where several technologies have been introduced. Driven initially by the need to increase durability, the industry went from the traditional cast iron manifolds to stainless steel tubular or clamshell designs with or without heat insulation such as air gaps. Manifold design must consider various imperatives and constraints which generally lead to a compromise among contradictory requirements. Amongst them are high durability standards, low emissions, minimised heat dissipation during cold-starting, maximised heat dissipation in high temperature conditions to minimise catalyst ageing and minimising mass in order to improve fuel economy.

Noxious emissions are effectively controlled by the adoption of a three-way catalytic converter. However, the catalytic converter will not be able to function effectively until it reaches the light-off or operating temperature which is in the region of 250-340°C as reported by Burch et al. (1995). Recent research has revealed that 60-80% of the unburned HC are emitted from a motor vehicle equipped with a catalytic converter within the first few minutes following an engine cold-start. This offers scope for the reduction of overall engine emissions; in particular where short, urban driving is done.

Typically, adequate physical testing of new manifolds is at best lengthy and expensive and, at worst, completely cost prohibitive and often incapable of providing a complete understanding of its performance. Hence, relying solely on physical testing may not provide all the necessary data as engineers may not gain enough timely information to make the best product development decisions. It is also often difficult to repeat standard tests and achieve consistent results. With an ever-increasing need to accelerate development, trace design decisions, and optimise design performance within acceptable tolerances, the requirement to leverage design simulation tools has grown.

To reduce the time spent on experiments and optimisation studies for improved catalyst light-off, many works on modelling have been conducted along with experiments. Some simulation studies focused on predicting the conversion behaviours of the catalytic converters and their design optimisation, while others studied the prediction of the thermal response of the

exhaust gas in the air-gap dual pipe exhaust system to improve exhaust pipe design for thermal energy preservation (Liu et al., 1995 & Konstantinidis, Koltsakis and Stamatelos, 1997). Baba et al. (1996) employed a two-dimensional (2-D) simulation model to investigate the effects of loading quantities of the noble metals for improved catalyst conversion efficiency. Yasgashi et al. (1994) applied a simulation technique to optimise the heating pattern of an electrically heated catalyst. Koltsakis et al. (1997), as cited by Chan and Hoang (1999), developed a 2-D catalytic converter model to investigate the effects of operating conditions such as gas flow pattern and catalyst ageing on the catalyst performance. These studies have separately studied thermal response of the exhaust gas in the manifold with constant inlet gas parameters. However, none of the above models consider the engine cold-start conditions on catalyst light-off where the wall temperatures of the manifold are gradually heated up by the exhaust gas. Such studies have only begun to appear rather recently (Chan & Hoang, 1999).

Furthermore, modelling of cold-start thermal response of the manifold is not simplistic as it involves complicated heat transfer processes which are governed by complex interactions between exhaust gas flow and the manifold itself. CFD is a powerful tool for such simulations. However its applicability for transient simulations is limited by high CPU demands (Tsinoglou et al., 2004).

The present study proposes an alternative computational method for the prediction of transient temperature fields in an exhaust manifold. Fig. 1 depicts the exhaust system of the 4-cylinder Ford engine under investigation. The objective of this paper is to develop a relatively simple FE model to compare the impact of the thermal properties of an engine's exhaust manifold on the manifold's exterior temperature during a cold start, in the absence of CFD software. Within this framework, it was decided to benchmark a cast stainless steel manifold of exactly the same configuration (geometry and dimensions) as the original Ford Rocam cast iron manifold, with the wall section reduced to 2.5 mm in both cases. Both cases were produced by the casting process. This numerical comparison may provide some indication in terms of the catalyst light-off time although the objective is not to quantify the difference in terms of actual time taken to reach light-off, but rather to qualitatively indicate the potential effect of the thermal properties of different manifold materials.

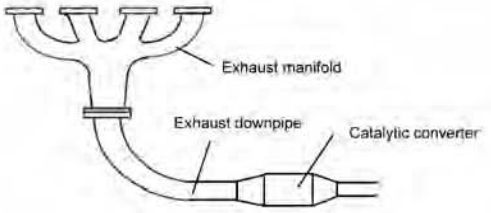

Figure 1: Schematic layout of exhaust system

2. HEAT TRANSFER MODES IN THE EXHAUST MANIFOLD AND THEIR RELATIVE IMPORTANCE

Heat transfer phenomena during engine cold-start are complicated as they involve liquid and vapour phases. When an engine is cold-started, the water vapour present in the hot exhaust gas is condensed onto the cold inner surface of the exhaust pipe forming a thin water film layer, which is subsequently evaporated when the gas temperature is in thermal equilibrium with the manifold temperature. The wet surface acts as a medium for heat transfer from the exhaust gas to the pipe wall. The condensation and evaporation occur simultaneously and ceases when the manifold wall temperature exceeds the dew point temperature of the water vapour. These processes are beyond the scope of the present study.

The exhaust gas flowing through the manifold will be cooled before reaching the catalytic converter as heat will be transferred from the exhaust gas to the manifold by forced convection and radiation, and dissipated via the following processes:

a) A portion of the heat transferred by the gas will be stored in the material, the importance of which will depend on the thermal mass (mass × specific heat). This amount of heat energy will be close to zero once the exhaust system has reached thermal equilibrium (fully warmed up).

b) The remaining portion of the heat transferred by the gas will be transmitted to the environment by radiation and possibly by free or forced convection, depending on the exhaust system's architecture. This portion of heat energy is initially very small but becomes more significant once the system reaches high temperatures. Under steady-state conditions, heat radiation will be the dominant mode of heat dissipation.

The heat loss by the exhaust gas to the manifold wall will reduce the catalyst temperature, which will in turn extend catalyst light-off time. However, losing heat facilitates the minimisation of catalyst ageing but will contribute to an increase in the under-bonnet temperature. Hence, it is desirable to minimise the heat loss right after cold-starts but maximise the heat loss at high load to minimise catalyst ageing.

3. MATHEMATICAL MODELS OF HEAT TRANSFER IN EXHAUST MANIFOLD

The flow in the exhaust pipe and its associated heat transfer modes are shown schematically in Fig. 2. Since the actual flow in the pipe is unsteady and compressible, the flow condition at any point of interest may be described by three independent variables, i.e. pressure, velocity and density. However, as the focus of the current study is on the thermal effects on the exhaust system on a comparative basis, the effect of flow pulsation due to pressure

wave actions acting on the heat transfer process is neglected.

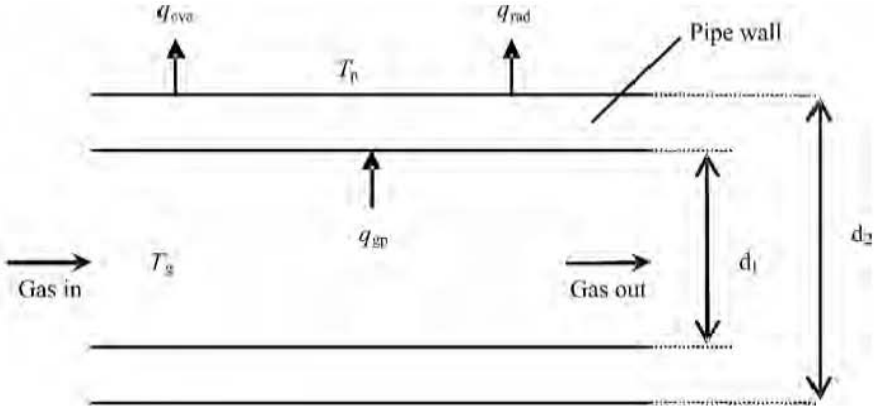

Figure 2: Schematic illustration of heat transfer modes

Three laws govern mass and heat flow: the laws of conservation of mass, conservation of momentum and conservation of energy. The conservation of mass is expressed by the equation of continuity, which for steady incompressible flow is

$$\nabla \cdot v = 0 \tag{1}$$

where v is the velocity of the fluid. Conservation of momentum is expressed by the momentum equation, which for the same conditions may be represented by

$$\rho \frac{dv}{dt} = -\nabla \rho + \eta \nabla^2 v + \mathbf{J} \times \mathbf{B} + \rho \mathbf{g} \tag{2}$$

where ρ is the mass density, t the time, η the viscosity, g the gravitational acceleration and $\mathbf{J}$ and $\mathbf{B}$ represents the Lorentz forces. Conservation of energy, neglecting Joule heating and viscous energy dissipation, is expressed by the energy equation as

$$\rho C_p \frac{\partial T}{\partial t} = k \nabla^2 T - \rho C_p (v.\nabla) T - \nabla . q_r \tag{3}$$

where C_p is the specific heat capacity at constant pressure, k the thermal conductivity, q_r the rate of heat or energy flow and T the temperature. By assuming a quasi-steady, incompressible flow, the 1-D energy equation for the exhaust gas and pipe wall may be represented as

$$\frac{\partial T_p}{\partial t} = \alpha \frac{\partial^2 T_p}{\partial x^2} + \frac{q_{gp} - q_{eva} - q_{rad}}{\rho_p c_p V_2} \tag{4}$$

Eq. (4) is actually the unsteady heat conduction equation with a uniform thermal conductivity applied to the pipe wall. The spatial and temporal temperature distribution $T(x,y,z,t)$ for 3-D heat conduction in a domain D is given as:

$$\frac{\partial}{\partial x}\left(\kappa_x \frac{\partial T}{\partial x}\right)+\frac{\partial}{\partial y}\left(\kappa_y \frac{\partial T}{\partial y}\right)+\frac{\partial}{\partial z}\left(\kappa_z \frac{\partial T}{\partial z}\right)+Q=\rho c\left(\frac{\partial T}{\partial t}-V\frac{\partial T}{\partial x}\right) \quad (5)$$

where Q is the power generation per unit volume and (x,y,z) the coordinate system.

3.1. Heat convection from exhaust gas to manifold wall

This mode of heat transfer is mainly due to forced convection and is strongly dependent on the gas flow dynamics and the manifold geometry. Neglecting the water film layer on the inner wall of the pipe due to quenching of the hot exhaust gas during engine cold-start, the heat flux may be expressed as

$$q=h_{gp}\left(T_g-T_p\right) \quad (6)$$

where h_{gp} is the convective heat transfer coefficient between the exhaust gas and the pipe wall, and is determined by

$$h_{gp}=N_u\frac{k}{d_1} \quad (7)$$

where k is the thermal conductivity of the gas, N_u the Nusselt number and d_1 the pipe inner diameter. The widely used Nusselt correlation, neglecting pipe bend and gas pulsation factors, proposed by Gnielinski (1976) and Mills (1999), was used for the present study.

For $0.5 < Pr < 2000$ and $10^4 < Re_D < 5\times10^6$,

$$N_u=\frac{\left(f/8\right)\left(Re_D-1000\right)Pr}{1+12.7\left(f/8\right)^{1/2}\left(Pr^{2/3}-1\right)} \quad (8)$$

where for non-smooth pipes, the friction factor f is given by

$$\frac{1}{\sqrt{f}}+2\log\left(\frac{\varepsilon}{3.7d}+\frac{2.51}{Re\sqrt{f}}\right)=0 \quad (9)$$

and Pr may be expressed as

$$Pr=\frac{C_p\mu}{k} \quad (10)$$

Reynolds number R_{e_D} may be computed from

$$R_{e_D} = \frac{4\dot{m}}{\pi\, d_1\, \mu} \tag{11}$$

3.2. Heat convection from pipe surface to ambient air

The heat flux from the pipe outer surface to the ambient air q_{cv} due to free convection is

$$q_{\text{cva}} = h_{\text{cva}}\left(T_{\text{p}} - T_{\text{a}}\right) \tag{12}$$

where

$$h_{\text{cva}} = \frac{N_u k_{\text{a}}}{d_2} \tag{13}$$

The Nusselt number is determined from the correlation proposed by Churchill and Chu (1975) as cited by Incropera and De Wit (1990) and is represented as

$$N_u = 0.6 + \left(\frac{0.387 Ra^{1/6}}{\left[1 + (0.599/Pr)^{9/16}\right]^{8/27}} \right) \tag{14}$$

where

$$Ra = \frac{l^3 g\beta \left(T_{\text{p}} - T_{\text{a}}\right)}{\nu_{\text{a}}^2} Pr \tag{15}$$

and the wetted length

$$l = \pi\, d_2 \tag{16}$$

The volumetric thermal expansion coefficient is evaluated at T_a while the other properties are evaluated at the film temperature T_f which may be calculated from

$$T_{\text{f}} = T_{\text{p}} - 0.38\left(T_{\text{p}} - T_{\text{a}}\right) \tag{17}$$

3.3. Heat radiation from pipe surface to surroundings

Heat loss due to thermal radiation between the manifold surface and environment is modeled by the standard Stefan-Boltzmann relation

$$q_{rad} = \varepsilon \sigma \left(T_p^4 - T_a^4 \right) \quad (18)$$

4. NUMERICAL MODELS OF HEAT TRANSFER IN EXHAUST MANIFOLD

In this work, a 3-D finite element model for simulating the heat transfer process in the exhaust manifold of a typical sedan vehicle using the ABAQUS commercial FEA code is developed. Appropriate convective and radiative boundary conditions are considered.

This section describes the basic energy balance, constitutive models, boundary conditions, finite element discretisation, and time integration procedures used.

4.1. Energy balance

According to the ABAQUS Theory Manual (2004), the basic energy balance is defined as

$$\int_V \rho \dot{U} \, dV = \int_V r \, dV + \int_S q \, dS \quad (19)$$

where V is the volume of solid material, with surface area S; $\dot{U}$ is the material time rate of the internal energy; and r is the heat supplied externally into the body per unit volume.

It is assumed that the problem is uncoupled in the sense that $U = U(T_p)$ only, and q and r do not depend on the strains or displacements of the body. For simplicity a Lagrangian description is assumed, so "volume" and "surface" mean the volume and surface in the reference configuration.

4.2. Constitutive definition

This relationship is written in terms of a specific heat and is given by

$$C_p \left(T_p \right) = \frac{dU}{dT_p} \quad (20)$$

Heat conduction is governed by the Fourier law and may be represented by

$$\mathbf{f} = -\mathbf{k} \frac{\partial T}{\partial \mathbf{x}} \quad (21)$$

where **f** is the heat flux and **x** the position.

4.3. Boundary conditions

Boundary conditions are specified as surface convection and radiation as described by Eqs (13)and (18), respectively

$$q_{\text{rad}} = A\left(T_p - T^z\right)^4 - \left(T_p^0 - T_p^z\right)^4 \tag{22}$$

where A is the radiation constant (emissivity times the Stefan-Boltzmann constant) and T^z is the absolute zero on the Kelvin scale.

4.4. Spatial discretisation

The variational statement of the energy balance, Eqs (19) and (21), is obtained directly by the standard Galerkin approach and is written as

$$\int_V \rho \dot{U} \delta T_p \, dV + \int_V \frac{\partial \delta T_p}{\partial \mathbf{x}} . \mathbf{k} . \frac{\partial T_p}{\partial \mathbf{x}} \, dV = \int_V \delta T_p \, r \, dV + \int_{S_q} \delta T_p \, q \, dS \tag{23}$$

where δT_p is an arbitrary variational field satisfying the boundary conditions. The manifold is geometrically approximated with finite elements, so that the temperature is interpolated as

$$T_p = N^N(\mathbf{x}) T_p^N, \qquad N = 1, 2, 3... \tag{24}$$

where N is the interpolation function and T_p^N the nodal temperatures.

3-D second-order polynomials are used for N^N. With these interpolations the variational statement described by Eq. (23) can be written as the system equation as

$$\int_V N^N \rho \dot{U} \, dV + \int_V \frac{\partial N^N}{\partial \mathbf{x}} . \mathbf{k} . \frac{\partial T_p}{\partial \mathbf{x}} \, dV = \int_V N^N \, r \, dV + \int_{S_q} N^N \, q \, dS \tag{25}$$

This set of equations is the "continuous time description" of the geometric approximation.

4.5. Time Integration

Abaqus/Standard uses the backward difference algorithm (Euler method or modified Crank-Nicholson operator) defined as

$$\dot{U}_{t+\Delta t} = \left(U_{t+\Delta t} - U_t\right)\left(1/\Delta t\right) \tag{26}$$

where Δt is the time increment.

Although the central difference method, which is used in other FEA codes, has the highest accuracy, it tends to produce oscillations in the early time solution. This problem is however not present in the backward difference form. The modified Newton method, including Jacobian contributions of conduction, radiation and convection, is expressed as

$$\left[\frac{1}{\Delta t}\int_V N^N \rho \left.\frac{dU}{dT_p}\right|_{t+\Delta t} N^M dV + \int_V \left.\frac{\partial N^N}{\partial \mathbf{x}}.\mathbf{k}\right|_{t+\Delta t} .\frac{\partial N^M}{\partial \mathbf{x}} dV + \int_S N^N \left(\frac{\partial h}{dT_p}\left(T_p - T_p^0\right) + h + 4AT_p^3\right) N^M dS\right] \bar{c}^M$$

$$= \int_V N^N r\, dV + \int_{S_q} N^N q\, dS - \frac{1}{\Delta t}\int_V N^N \rho \left(U_{t+\Delta t} - U_t\right) dV - \int_V \frac{\partial N^N}{\partial \mathbf{x}}.\mathbf{k}.\frac{\partial T_p}{\partial \mathbf{x}} dV \qquad (27)$$

where $T^N_{t+\Delta t, i+1} = T^N_{t+\Delta t, i} + \bar{c}^N$, i = iteration number

The integration procedure used in ABAQUS for transient heat transfer analysis procedures introduces a relationship between the minimum usable time increment and the element size and material properties. This is necessary in order to avoid spurious oscillations due to small time increments with second-order elements. The following equation is used as a guideline

$$\Delta t => \frac{\rho c_p}{6k}\Delta l^2 \qquad (28)$$

5. FINITE ELEMENT REALISATION

5.1. Application description and geometry

This work examines the thermal transient behaviour of an exhaust manifold and its downpipe (manifold assembly) during a cold-start. The problem domain comprises a Ford Rocam exhaust manifold and downpipe subjected to isothermal exhaust gas flow. A CAD model of the physical manifold, suitable for FEA, was developed from the IGES surface data. The actual geometry and complexity of the physical manifold was retained. The CAD model is depicted in Fig. 3.

Figure 3: Solid model of exhaust manifold with downpipe

5.2. Material model

Transient heat transfer analysis requires specification of thermal conductivity, specific heat, film coefficients and material density. Generally, the thermal response of steel and cast iron varies over its temperature range resulting in non-linear behaviour. However, material properties for cast iron (SiMo) at elevated temperatures are currently limited. Based on the data available, the following temperature-dependent, thermo-physical material properties, shown in Fig. 4, were used.

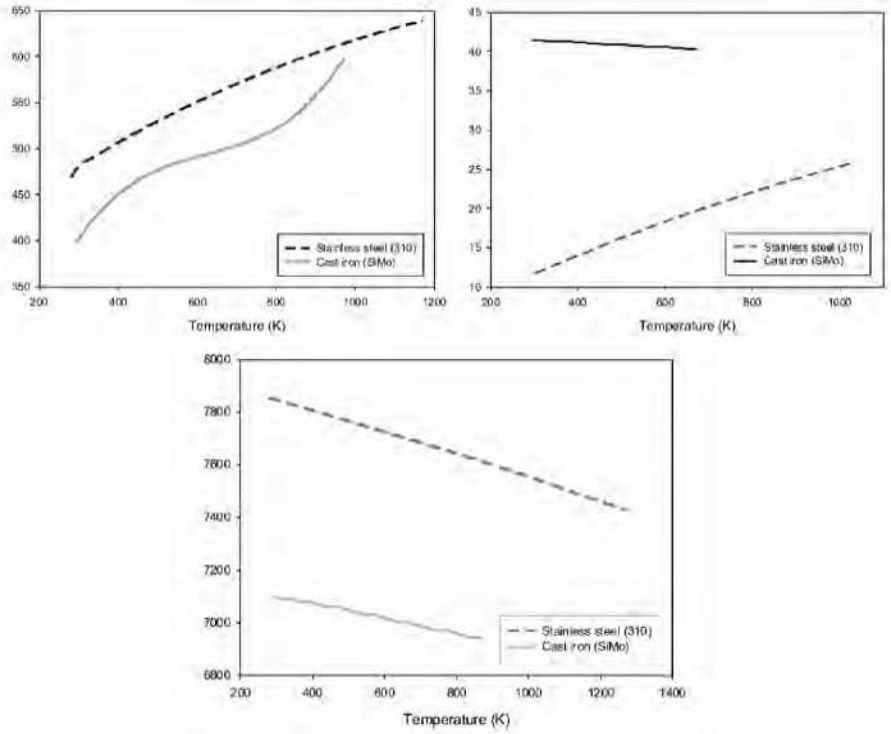

Figure 4: Thermo-physical properties of stainless steel (310) and cast iron (SiMo)

5.3. Boundary conditions and loading

The outside surface of the manifold is exposed to air that has a constant temperature of 300 K. A total mass flow rate of 0.033 kg/s with gas inlet temperature of 473 K was used. The initial temperature was set to 300 K in the entire model. No temperature boundary conditions were applied. The thermal response of the model is driven entirely by thermal loading through film coefficients.

5.4. Interactions

The inner manifold surfaces are in contact with the exhaust gas. Heat flux on the inner manifold surfaces is applied by a film condition as depicted in Fig. 5. Using the equations described in section 3 together with an internal surface roughness value of 0.26 mm (Mills, 1999) introduced by the fabrication process (investment casting) to calculate the relevant friction factor, the heat transfer coefficient (neglecting entrance, pipe bend and pulsation factors) was analytically computed as approximately 199.12 W/m^2/K. Similar values were reported by Zidat and Parmentier (2003). The outer surfaces, initially associated with a sink temperature of 300 K, are exposed to free air, which has a film coefficient of 15 W/m^2/K. Emissivities of 0.2 and 0.8 were prescribed for stainless steel and cast iron, respectively.

Figure 5: Manifold assembly subjected to heat flux

5.5. FE Mesh Details

Due to the complexity of the model, a global mesh seed of size 5 mm was assigned. Second-order tetrahedral diffusive heat transfer elements were used to discretise the manifold assembly. Due to the prevailing unstructured mesh, TET 10 elements of type DC3D10 were employed. The size of the model was in the region of 186 000 degrees of freedom. The mesh was checked in terms of standard mesh quality protocols. No mesh adaptive meshing was used due to computational costs. The finite element mesh is depicted in Fig. 6 below.

Figure 6: FE representation of the manifold assembly

6. RESULTS AND DISCUSSION

Figs. 7 and 8 show the temperature distribution of the exhaust manifold at 40 s. The simulation of the steel model converged at 7.78 hrs of CPU time in 103 increments while the cast iron model converged at 10.32 hrs of CPU time in 103 increments.

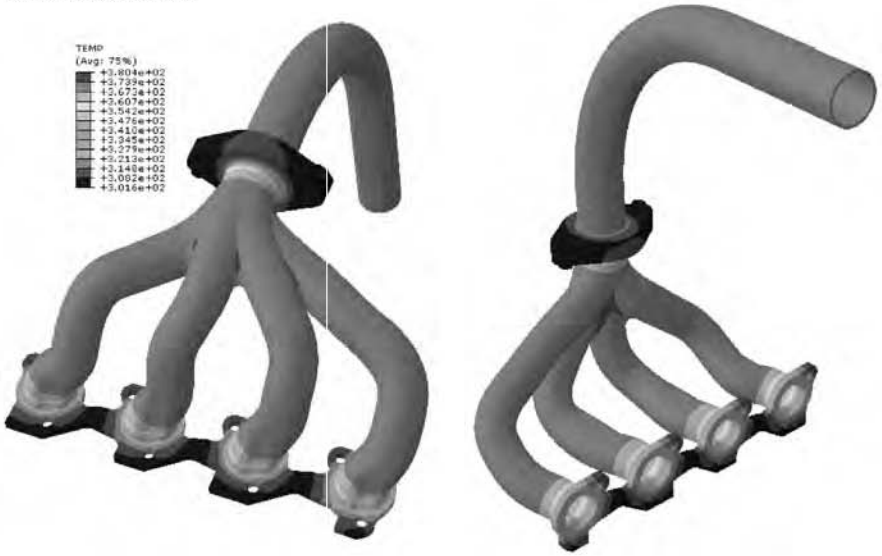

Figure 7: Temperature distribution in steel manifold assembly at 40 s in Kelvin

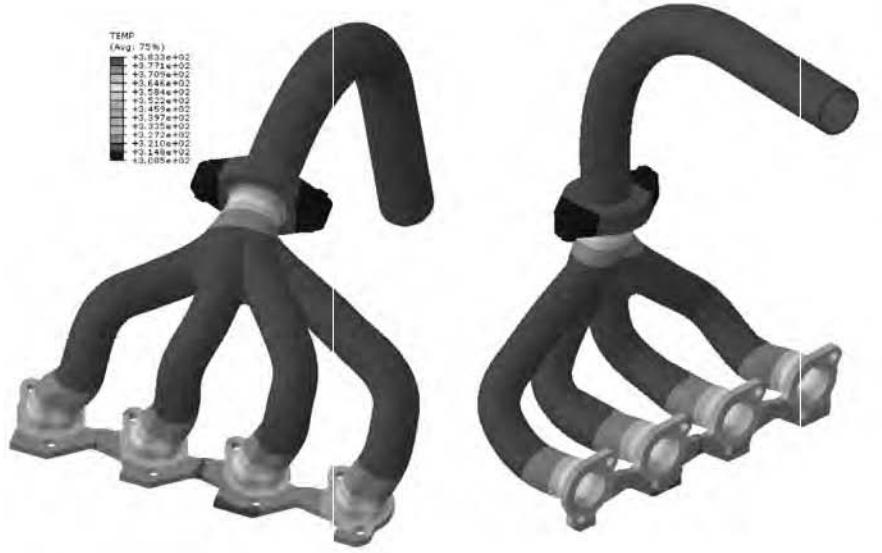

Figure 8: Temperature distribution in cast iron manifold at 40 s in Kelvin

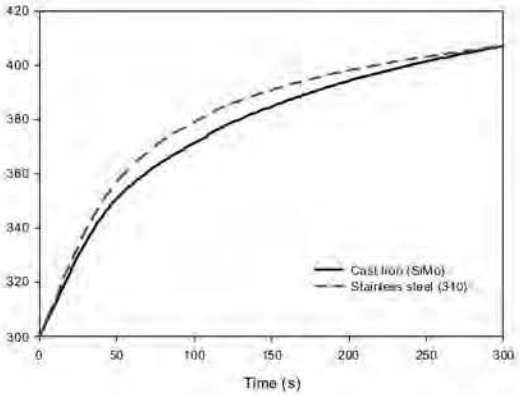

Figure 9: Comparison of manifold temperature evolution at arbitrarily chosen exterior reference point

The magnitude of the nodal temperatures at the specified reference point as a function of time is shown in Fig. 9. The profile generated is similar to actual experimental measurements performed by De Rouw (2007) both in trend and values and to findings reported by Galindo et al. (2006). Differences between this comparison to what is normally expected (other manifolds) can be attributed to various factors such as: availability of non-linear material property data, use of constant emissivities, gas properties and heat transfer coefficients, differences in wall thickness, manifold geometry and surface roughness values, neglecting pipe bend, entrance and gas pulsation factors, manifold material, inlet conditions and finally, differences in measurement locations. It is important to note that this numerical comparison may provide some indication in terms of the catalyst light-off time although the objective is not to quantify the difference in terms of actual time taken to reach light-off, but rather to qualitatively indicate the potential effect of the thermal properties of different manifold materials. Furthermore, Fig. 9 is by no means indicative of the thermal behaviour of the entire manifold but rather at a specific measurement point.

The simulations reveal that both materials exhibit similar temperature profiles under the operating conditions described. Although cast iron has a higher thermal conductivity than steel, the results, based on the contour plots at 40 seconds, indicate that the cast iron manifold has only a slightly higher overall outer wall temperature than the steel manifold. This may be due to the significant difference in emissivities between the two materials and to the heat transfer modes of conduction and surface radiation competing in a complicated way. This implies that contrary to popular opinion, a material having a higher thermal conductivity does not necessarily dominate the surface temperature distribution. It has been shown that the surface temperature distribution depends on many competing factors with the internal heat transfer coefficient being the most dominant mode of heat loss from the manifold.

7. CONCLUSIONS AND RECOMMENDATIONS

The transient thermal performance of an exhaust manifold is governed by complex interactions between the exhaust gas flow and the manifold itself. CFD is a powerful tool for such simulations and has therefore been widely used in previous research works. However, its applicability is usually limited to steady-state simulations, due to the high computational times involved in transient CFD simulations.

The present study proposes an alternative computational method for the simulation of transient heat transfer in an exhaust manifold assembly. The objective of this simulation is to assess and rank the relative impact of the manifold's thermal properties on its exterior temperature. It was observed that the proposed equations and model can predict the temperature distribution within reasonable time. The results show that stainless steel manifolds potentially minimise heat loss from the exhaust gas when compared with their cast iron counterparts during a specific time increment. This may result in an increase in thermal energy being available to heat the catalyst.

Since thermal analysis is sensitive to temperature-dependent material properties and the current analysis involves limited properties for SiMo, it is recommended that the analysis be re-run as soon as more accurate material properties are made available.

Depending on the degree of accuracy required, it is further recommended that the developed model be refined and enhanced by employing user subroutines to accurately simulate temperature-dependent film boundary conditions.

It is believed that the proposed modelling procedures, developed heat transfer model and results presented would bring a greater understanding of the thermal behaviour of the exhaust manifold during a cold-start and would be of practical benefit in manifold design and analysis.

8. ACKNOWLEDGMENTS

The work described in this paper has been supported and funded by the Institute of Technology Innovation (IOTI), Tshwane University of Technology, South Africa. The author wishes to thank Dr Arthur Bell from Stellenbosch Automotive Engineering (Pty) Ltd (CAE) for providing the manifold CAD data, gas inlet data and general guidance for the simulation.

9. REFERENCES

ABAQUS. 2004. ABAQUS theory manual. Version 6.5. USA: Abaqus, Inc.

Baba, N, Ohsawa, K & Sugiura, S. 1996. Numerical approach for improving the conversion characteristics of exhaust catalysts under warming-up

condition. *Society of Automotive Engineers*, SAE paper 962076.

Burch, SD, Porter, TF, Keyser, MA, Brady, MJ & Michaels, KF. 1995. Reducing cold start emissions by catalytic converter thermal management. *Society of Automotive Engineers*, SAE paper 950409.

Chan, SH & Hoang, DL. 1999. Heat transfer and chemical reactions in exhaust system of a cold-start engine. *International journal of heat and mass transfer,* 42: 4165-4183.

Churchill, SW & Chu, HHS. 1975. Correlating equations for laminar and turbulent free convection from a horizontal cylinder. *International journal of heat and mass transfer,* 18: 1049-1053.

De Rouw, B. 2007. Comparison of thermal properties of thin walled stainless steel exhaust manifolds with standard cast iron, *CAE report* , project file AAB481, 1-12.

Galindo, J, Lujan, JM, Serrano, JR, Dolz, V & Guilain, S. 2006. Description of a heat transfer model suitable to calculate transient processes of turbocharged diesel engines with one-dimensional gas-dynamic codes. *Applied thermal engineering,* 26: 66-76.

Gnielinski, V. 1976. *Institute of Chemical Engineers*, 16.

Incropera, FP & De Witt, DP. 1990. *Introduction to heat transfer.* 2nd ed., John Wiley & sons, Inc.

Koltsakis, GC, Konstantinidis, PA & Stamatelos, AM. 1997. Development and application range of mathematical models for 3-way catalytic converters. *Applied Catalysis B: Environmental,* 12: 161-191.

Konstantinidis, PA, Koltsakis, GC & Stamatelos, AM. 1997. Transient heat transfer modelling in automotive exhaust systems. *Institution of Mechanical Engineers*, 211, Part C.

Liu, Z, Hoffmanner, AL, Skowron, JF & Miller, MJ. 1995. Exhaust transient temperature response. *Society of Automotive Engineers*, SAE paper 950617.

Mills, AF. 1999. *Basic heat and mass transfer.* 2nd ed., Prentice Hall, New Jersey.

Tsinoglou, DN, Koltsakis, GC, Missirlis, DK & Yakinthos, KJ. 2004. Transient modelling of flow distribution in automotive catalytic converters. *Applied mathematical modelling,* 28: 775-794.

Yasgashi, T, Yoshizake, K, Nagami, T, Sugiura, S, Yoshimaga, T & Ohsawa, K. 1994. New technology for reducing the power consumption of electrically heated catalysts. *Society of Automotive Engineers*, SAE paper 940464.

Zidat, S & Parmentier, M. 2003. Exhaust manifold design to minimize catalyst light-off time. *Society of Automotive Engineers*, SAE paper 2003010940.